Design and Development Status of MKID Integral Field Spectrographs for High Contrast Imaging

Seth R. Meeker[a], Benjamin A. Mazin[a], Rebecca Jensen-Clem[b], Alex B. Walter[a], Paul Szypryt[a], Matthew J. Strader[a], and Clint Bockstiegel[a]

[a]Department of Physics, Univ. of California Santa Barbara, Santa Barbara, CA, USA
[b]Department of Astronomy, California Institute of Technology, Pasadena, CA, USA

ABSTRACT

We report on the design and development progress of two Microwave Kinetic Inductance Detector (MKID) integral field spectrographs (IFSs) for high-contrast astronomy applications. DARKNESS is a 10,000 pixel MKID IFS that will integrate with the coronagraphs at Palomar Observatory, as well as directly with the Palm-3000 (P3K) extreme adaptive optics (AO) system. MEC is a 20,440 pixel MKID IFS that will integrate with the Subaru Coronagraphic Extreme AO (SCExAO) system at the Subaru Telescope. Both IFSs are optimized for 700 to 1400 nm bandpasses to provide low resolution spectroscopy across I and J bands. MKIDs are a promising technology for overcoming the current contrast ceiling in coronagraphic instruments imposed by atmospheric speckles that vary on 1-second timescales. These speckles vary too slowly to average out with long exposures, and too quickly to control in real time with conventional focal plane detectors or to subtract reliably with differential imaging. With these instruments we will demonstrate how the high time resolution of MKIDs allows focal plane speckle nulling at the speed necessary to control atmospheric speckles in real time, and discrimination of speckles from faint companions during post-processing using statistical techniques similar to the "dark speckle" approach. Additionally, the energy resolution of MKIDs allows either form of speckle suppression to be applied as a function of wavelength. First-light for DARKNESS is scheduled for July 2016 and first-light for MEC is targeted for Fall 2016/Winter 2017.

Keywords: instrumentation: adaptive optics, instrumentation: detectors, instrumentation: high angular resolution, planetary systems

1. INTRODUCTION

The field of high-contrast imaging is young and expanding rapidly with dedicated high-contrast instruments that pair coronagraphy with extreme AO, such as Project 1640 (P1640),[1] GPI,[2] SPHERE,[3] and SCExAO,[4] only recently coming online. The contrast ceiling achieved by these instruments is currently set by speckles (scattered residual starlight that escapes coronagraphic suppression and interferes coherently in the final image plane) that vary on timescales too fast to subtract with differential imaging, but too slow to average down efficiently (see discussion in Section 3.1.1 of Jovanovic et al.[5]). Overcoming this barrier requires speckle control at very high frame rates, necessitating the development of fast, low-noise, near-infrared focal plane detectors. In this proceeding we present the design and development status of two instruments that aim to address this need: the DARK-speckle Near-infrared Energy-resolving Superconducting Spectrophotometer (DARKNESS) and the MKID Exoplanet Camera (MEC).

DARKNESS and MEC are unique among high-contrast imagers because of their Microwave Kinetic Inductance Detector (MKID)[6] focal plane arrays. MKIDs are an emerging low temperature detector technology that, through microwave multiplexing techniques and their inherently simple geometric design, enable relatively low-cost large (kilo- and potentially mega-pixel) arrays. Originally conceived for sub-millimeter astronomy applications, our group has developed MKIDs for UV, optical, and near-IR (UVOIR) wavelengths[7–10] and fielded the first MKID camera at any wavelength to produce published astronomical science results.[11–13] At these wavelengths MKIDs detect individual photons with time resolution of a few microseconds, are capable of measuring

Further author information: (Send correspondence to S.R.M) S.R.M.: E-mail: srmeeker@physics.ucsb.edu

individual photon energies to within a few percent, and have no analogue for the read-noise or dark current present in conventional semiconductor-based detectors. In the remaining introduction we will give a brief background of MKID technology and will highlight the speckle removal techniques enabled by MKIDs. In Section 2 we present the designs for DARKNESS and MEC and report on their current in-lab characterization. In Section 3 we present simulations of DARKNESS's expected performance and early science capabilities. In Section 4 we discuss the ongoing development of both instruments leading up to commissioning and beyond.

1.1 Microwave Kinetic Inductance Detectors

MKIDs operate on the principle that incident photons will briefly change the surface impedance of a superconductor through the kinetic inductance effect. The kinetic inductance effect is caused by the finite mass of the Cooper pairs (bound electrons) that make up the supercurrent. Reversing the supercurrent direction in an AC field requires the extraction of stored Cooper pair kinetic energy, which ultimately manifests as an additional surface inductance in the superconductor. When incident photons break Cooper pairs the superconductor's surface impedance (dominated by the kinetic inductance) changes, which can be measured by using the superconductor as a variable inductor in a resonant circuit. The change in surface impedance will shift the frequency of the resonance, which, in turn, causes a shift in the amplitude and phase of a microwave probe signal that is coupled to the circuit. See Figure 1 of Day et al.[6] for the canonical illustration of this operating principle. By fabricating individual resonators with different geometries (and thus different resonant frequencies) a single microwave transmission line (referred to later as the "feedline" for brevity) can read out thousands of resonators simultaneously through frequency domain multiplexing (FDM).[9]

Since the gap energy of a superconductor is very small (e.g. $\sim 10^{-4}$ eV for substoichiometric titanium nitride (TiN_x)), a high energy ($\sim$1 eV) optical photon will break many thousands of Cooper pairs, creating a "pulse" in the probe signal's phase as the resonator moves off-resonance rapidly (in $\sim$1 μs) upon absorbing the photon, then decays back to its steady state more slowly (in $\sim$50 μs) according to the quasiparticle lifetime. Examples of these pulses can be seen in Section 2.2.1. The sharpness of the pulse rise-time, combined with the continuous readout of every resonator simultaneously, provides the high time resolution of MKIDs. Photons with higher energies will break a greater number of Cooper pairs, creating phase pulses with magnitudes proportional to photon energy. This provides the intrinsic energy resolution of MKIDs.

1.2 Speckle Discrimination Techniques with MKIDs

1.2.1 Spectral Differential Imaging

With the spatial and spectral information provided by an IFS one can take advantage of the chromatic nature of the speckle pattern to perform Spectral Differential Imaging (SDI or spectral deconvolution).[14] Speckles move away from the center of the focal plane when observed at longer wavelengths, while astrophysical sources will remain in-place. The most straightforward method to exploit this speckle diversity is to take exposures at two different wavelengths, scale them in size to align the speckle patterns, and subtract the two images to remove the speckles.[15] However, modern algorithms incorporate all spatial-spectral information into a single analytical framework employing principle component analysis (PCA) to build a model of the speckle pattern and detect faint companions.[16]

1.2.2 Statistical Speckle Discrimination

The intensity of an astrophysical point source follows Poissonian statistics, whereas speckle intensities follow a modified Rician (MR) distribution.[17,18] Dark Speckle imaging[19–21] and Stochastic Speckle Discrimination (SSD)[22,23] are examples of post-processing techniques that exploit these underlying statistics to distinguish faint companions from speckles. In the Dark Speckle technique destructive interference in the speckle pattern will create regions in the focal plane that register zero photon counts during a short exposure, unless a companion is present at that location, which decreases the likelihood of measuring zero photons. In SSD the absolute intensity level is not as relevant as the shape of the intensity distribution at each location. A MR distribution should have positive skewness, but if a companion is also contributing intensity the distribution shape is noticeably altered. To optimally take advantage of either technique requires an instrument with photon counting or fast framing capabilities to expose faster than the shortest speckle lifetimes without dark current or read noise that would affect the intensity statistics.

1.2.3 Focal Plane Wavefront Control

Coherent differential imaging (CDI) is performed by modulating speckles during observation using the deformable mirror (DM) of the AO system, actively creating speckle diversity to distinguish them from faint companions whose light is incoherent with the speckles. By applying the modulation in a closed-loop, using the focal plane image to feedback to the DM, speckles can be actively nulled during observation.[24] While speckle nulling has been demonstrated on sky,[5,25] performance behind a ground-based AO system is limited by the focal plane detector speed. To operate at the rates necessary to overcome atmospheric speckles and avoid AO lag requires detectors with frame rates >1 KHz.

2. DARKNESS & MEC OVERVIEWS

DARKNESS is a 10,000 pixel MKID IFS that will integrate with Project 1640 (P1640) and the Stellar Double Coronagraph (SDC) at Palomar Observatory, as well as directly with the Palm-3000 (P3K) extreme AO system. MEC is a 20,440 pixel MKID IFS that will integrate with the Subaru Coronagraphic Extreme AO (SCExAO) system at the Subaru Telescope. Both IFSs are optimized for 700 to 1400 nm bandpasses to provide low resolution spectroscopy across I and J bands. Below we provide overviews of both instruments including cryostat design and performance, MKID development, and readout design.

2.1 Cryostats

DARKNESS's cryostat is a liquid cryogen pre-cooled Adiabatic Demagnetization Refrigerator (ADR) capable of reaching temperatures below 100 mK. A liquid cryogen design was selected due to space constraints in the Hale Telescope Cassegrain cage, preventing the use of pulse tube cooling. It is designed as a drop-in replacement for PHARO[26] and the P1640 IFS.[27] With this in mind, DARKNESS's custom cryostat inherits its basic shape from these existing instruments, but has a rectangular bottom plate and is 8.4 inches taller than PHARO to accomodate more cryogen volume. The 300 K enclosure measures roughly 25 inches long × 13 inches wide × 23.5 inches tall (27.17 inches tall including connections to the bottom plate). Internally DARKNESS has two radiation shields, one at 77 K and one at 4 K. In the lab we measure a 77 K hold time (with 8 liters of LN2) of 36 hours and a 4 K hold time (with 22 liters of LHe) of 40 hours. Figure 1 shows several photographs of the cryostat with views of the inner stages.

MEC's cryostat is an off-the-shelf pulse-tube cooled ADR cryostat, so we will not provide detailed figures or descriptions here. Drawings and specifications can be found on HPD's website.* One important note: the pulse tube continuously cools the cryostat to 2.7 K, rather than 4 K. For brevity we will not make this distinction throughout the paper, but the reader should note that whenever the 4 K stage is mentioned, this is actually a 2.7 K stage in the case of MEC.

2.1.1 Detector Package/100 mK stage

In both cryostats the detector packages are mounted to the 4 K plate and enclosed in Amumetal magnetic shields. Carbon fiber support structures hold an intermediate 1 K stage above the 4 K base, and the 100 mK stage hangs from the 1 K stage by Vespel SCP-5050 suspension (See Figure 1d for an example of the detector package installed in DARKNESS). This design places the MKID array far from the magnetic shield opening where field leakage will be strongest, and also allows us to install a black baffle on the 1 K stage to further reduce off-axis scattered light and 4 K blackbody radiation. The 1 K and 100 mK stages are attached to the ADR unit by copper rods that penetrate throught the magnetic shield. The ADR acts as a single-shot magnetic cooler which brings the MKID array down to 100 mK where the temperature is stabilized with a feedback loop to the ADR magnet power supply. In DARKNESS we achieve a 100 mK hold time of ∼20 hours in the lab with the detector package and wiring installed. MEC's detector package and wiring have not yet been installed, but with a lower heat load than DARKNESS and ADR cooling starting from 2.7 K rather than 4 K we anticipate a final hold time >20 hours.

*www.hpd-online.com/102_cryostat.php

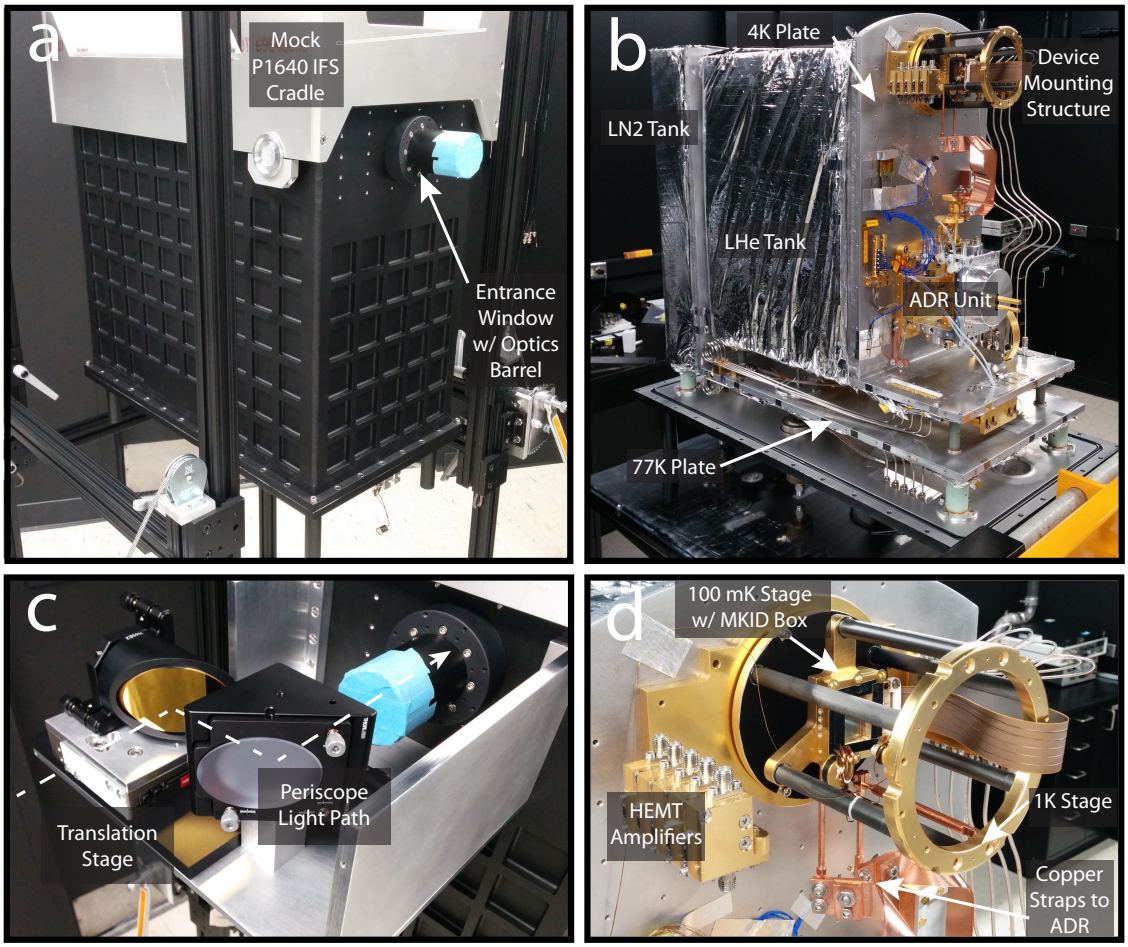

Figure 1. Photographs of the DARKNESS cryostat and internal structures. a) The DARKNESS cryostat hanging in its lab frame, including a mock P1640 IFS cradle. The 300 K shell is o-ring sealed at the bolt pattern visible along the base and is opened by lowering out the internal stages with a lift. The swappable magnifying optics barrel screws directly onto the cryostat entrance window. b) Internal view of cryostat with 300 K shell, 77 K shell, and 4 K shell removed. ADR unit is attached at bottom of 4 K plate and is connected to the 100 mK detector package with flexible copper straps. c) Periscope structure (Section 2.1.3) with enclosure sides removed. The periscope serves to reposition the incoming beam for DARKNESS's entrance window. By placing the first periscope mirror on a translation stage we can scan the field-of-view laterally over the detector. d) A zoomed-in view of the MKID detector package inside its mounting structure, including input signal cables (coax and flex cable) on the right side and HEMT amplifiers on the output side. The magnetic shield, 1 K baffle, and signal output cables have been removed for clarity. The 1 K stage sits atop three carbon fiber supports with the 100 mK stage hanging from it on three Vespel SCP-5050 supports.

2.1.2 Wiring

DARKNESS requires five feedlines to read out an entire array, and MEC requires ten. The layout of these signal paths is nearly identical for both instruments, just doubled for MEC. Hermetic SMA bulkhead connectors bring the signals into the cryostats, then stainless steel semi-rigid coax cables bring the signal to the 4 K stage where they are heat sunk to the 4 K plate with SMA feedthroughs. Inside the 4 K stage, hand-formable SMA-to-SMA coax bring the signal to the device mounting structure. On the device mounting structure, hand-formable SMA-to-G3PO coax connect to a superconducting NbTi flex cable, which brings the signal from the 4 K plate of the mounting structure to the 100 mK stage. An example of this flex cable is visible in Figure 1d and Figure 2 (Right). A full report of its design and performance is in preparation (Walter et al., in prep.). The flex cable connects to the MKID box with G3PO connectors allowing for a much more compact detector package than standard SMA connectors. The box-mounted G3PO connectors are solder connected to gold-plated copper on

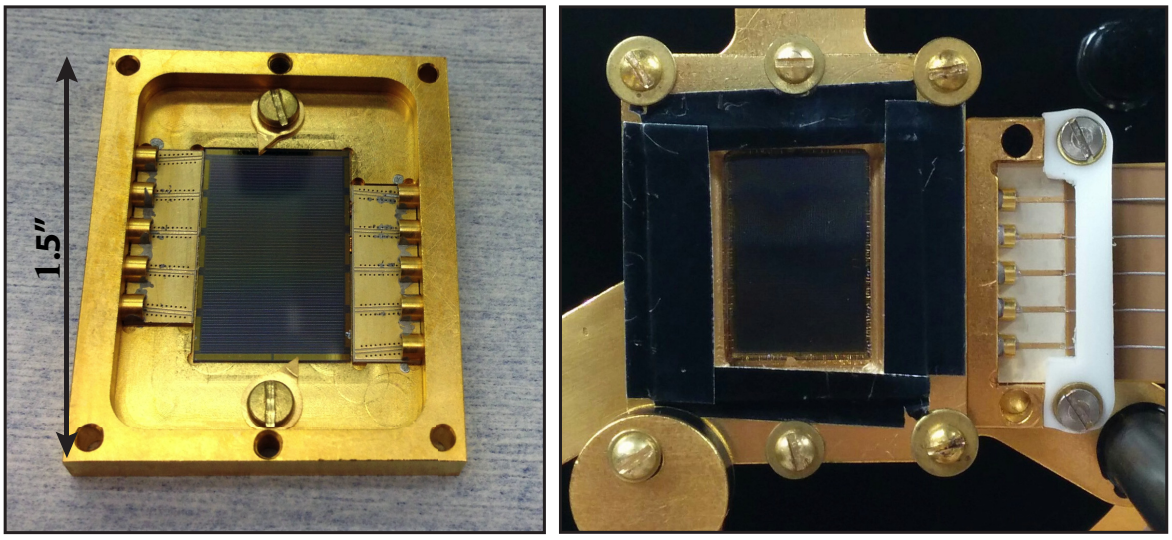

Figure 2. (Left) A 10,000-pixel D-1 array mounted in its microwave box (without box lid for clarity). The microwave signals are brought into the box through edge mount male G3PO connectors soldered to gold on duroid co-planar waveguide (CPW) transition boards, which are then connected to the MKID array with aluminum and gold wirebonds. (Right) Device box with lid, indium tin oxide coated window, and microlens array mounted in cryostat. The superconducting flex cable that brings microwave signals in to the box from the 4K stage is visible on the right (see Section 2.1.2. Identical output cable on left is disconnected in this photograph).

duroid CPW transition boards, which are then aluminum wire-bonded to the MKID chip (see Figure 2 (Left)). After passing through the MKID array the signals are brought out through the same series of CPW board, G3PO connectors, custom NbTi microstrip flex cable, and G3PO-to-SMA wires. At 4 K each line is amplified by a Low Noise Factory High Electron Mobility Transistor (HEMT) amplifier and the signals are taken to 300 K using the same combination of hand-formable and semi-rigid coax as the input side.

2.1.3 Optical Design

A key benefit of any MKID based IFS is the simplicity of the internal optics: no dispersive elements or cold reimaging optics are required for DARKNESS or MEC. Here we will walk through the few optical elements required.

Magnifying Optics: DARKNESS and MEC both have provisions for an interchangeable optics barrel that attaches directly to their entrance window holders and can be swapped with various magnifying optics to adjust the plate scales as necessary. In DARKNESS's baseline design we achieve Nyquist sampling of the P1640 focal plane by magnifying 2× using a pair of lenses, resulting in a plate scale of 25 milliarcseconds (mas) per 150 μm pixel. At this plate scale DARKNESS samples roughly half of the P1640 field-of-view (FOV). MEC's optical design has not been finalized yet, as the SCExAO backend is currently undergoing significant re-arrangement, but magnifying optics are not expected to be required.

Periscope: The entrance windows to the P1640 IFS and PHARO are off-center on the front face of their cryostats. However, if the beam entered DARKNESS at this same position, it would be obstructed by the cryostat's 4 K shell. To solve this we have designed a periscope setup that folds the beam with two 45° elliptical mirrors (see Figure 1c). By placing the first mirror on a high-precision translation stage we can scan the beam across the detector array. With the plate scale described above, this provides a simple way to select the half of the P1640 FOV of interest for each observation. MEC will also have provisions for the periscope, but is not expected to require it.

Cryostat Windows: The entrance windows of DARKNESS and MEC are 12.7 mm thick, $\lambda/20$ flatness, AR-coated Fused Silica windows. At the 77 K and 4 K stages we use 4mm thick N-BK7 windows. The 77 K window is AR-coated both sides, while the 4K window is AR-coated on the inner face and has a custom band-defining reflective filter deposited on the outer face. The 77 K and 4 K windows are both mounted at 10° angles relative to

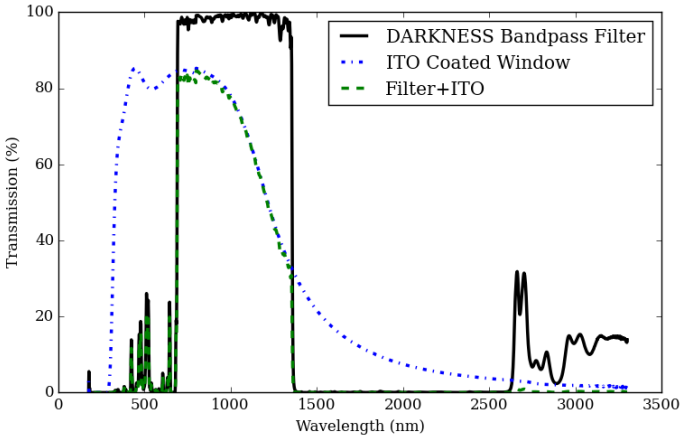

Figure 3. Transmission measurements of DARKNESS's IR blocking filters. We find the ITO filter encroaches severely on DARKNESS's science bandpass and are seeking alternative coatings or glasses to replace it.

the incoming beam in order to reduce ghosting. At 100mK the MKID box lid holds an Indium Tin Oxide (ITO) coated window for our final level of infrared radiation blocking. Transmission curves for both the band-defining filter and the ITO window are shown in Figure 3. Our previous studies of ITO coated windows were primarily concerned with IR blocking in ARCONS,[11] which has a science bandpass of 400 nm to 1100 nm where the ITO transmits well. We find the ITO filter we are accustomed to encroaches severely on DARKNESS's science bandpass and are seeking alternative coatings or glasses to replace it.

Microlens Array (MLA): The only cold powered optic required in DARKNESS and MEC is a MLA at the final focus to concentrate the beam onto the MKID inductors. We use a MLA from Advanced Microoptics Systems with radius of curvature equal to 0.8 mm, effective focal length of 0.95 mm (at 633 nm), and 90% fill factor, made from high index STIH53 glass.

2.2 MKID Array Design

The MKID arrays for DARKNESS and MEC will have identical pixel designs and fabrication processes, with the only difference being the number of feedlines and arrangement of the pixels on each feedline. Here we present results from a prototype 10,000-pixel near-IR optimized MKID array (known as D-1), which tests the general pixel design and fabrication techniques that will be shared by DARKNESS and MEC.

2.2.1 Pixel Design

Figure 4 shows a schematic of the base D-1 pixel design with key design parameters and material properties listed in Table 1. Resonators are capacitively coupled to the feedline with a coupling bar that runs along the bottom of the pixel's capacitor and serves as an extension of the coplanar waveguide (CPW) feedline's center strip. The length of this coupling bar controls the coupling quality factor, Q_c, of the resonator. The overall measured quality factor, Q_m, is set by Q_c and the internal quality factor, Q_i, according to the equation $1/Q_m = 1/Q_i + 1/Q_c$. For the resonators in D-1, Q_i is typically $> 10^5$ so Q_c dominates. D-1 pixels are designed for $Q_m \approx Q_c = 30{,}000$.

The overall MKID pixel size is determined by several competing factors including readout frequency, plate scale, and sensitivity, where sensitivity refers to the phase shift induced by a photon of a given energy. The fractional change in Cooper pair density within the inductor, $\delta N_{CP}/N_{CP}$, determines the MKID's frequency shift, which, when combined with the width of the resonance set by Q_m, determines the phase shift measured by the probe signal. For a given Q_m, the ratio $\delta N_{CP}/N_{CP}$ must be optimized to give the desired maximum phase shift from the highest energy photon the instrument will detect. The highest energy photon (and therefore δN_{CP}) is set by astronomical application, so the MKID sensitivity must be tuned by adjusting the inductor volume to control N_{CP}. Adjusting the volume by using a thinner film is not an option as TiN absorption drops off quickly for films thinner than $\sim$50 nm.[29] With inductor geometry set by this sensitivity argument, the pixel

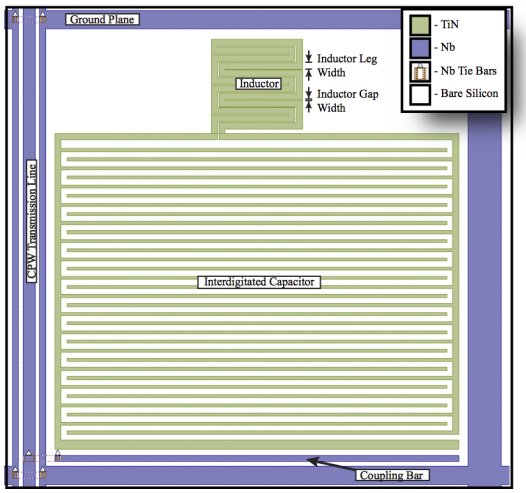

Table 1. D-1 MKID Design Parameters

Resonator Material	TiN
Superconducting Transition Temperature (T_c)	1 K
Resistivity (ρ_n)	110 $\mu\Omega$ cm
Film Thickness (t)	60 nm
Surface Inductance (L_s)	24 pH/sq
Inductor Width × Height	30 × 30 μm
Average Inductor Leg Width	2.5 μm
Inductor Gap Width	0.3 μm
Interdigitated Capacitor (IDC) Width × Height	133 × 104 μm
IDC Leg Width	1 μm
IDC Gap Width	2 μm
Total Kinetic Inductance (L_k)	5018 pH
Total Magnetic Inductance	182 pH
Total Capacitance	0.25 pF
Resonant frequency	4.41 GHz
Quality Factor ($Q = f/\Delta f_{FWHM}$)	30,000

Figure 4. Schematic of the D-1 base MKID design with key parameters listed in Table 1.
NOTE: L_s is calculated using Eqn.(47) from Zmuidzinas 2011[28] for the thin film limit, $L_s = \frac{\hbar}{\pi\Delta_0}\frac{\rho_n}{t}$ where $\Delta_0 = 1.764\, k_B T_c$ is the zero temperature value of the superconducting gap energy and ρ_n is obtained from a test TiN deposition. For a strip of superconductor with length l and width w, $L_k = L_s(l/w)$.

size and capacitor geometry are then tailored to achieve the desired resonant frequency (∼4.4 GHz for the D-1 base design) within a small enough area to allow for 10,000-20,000 pixels to fit on a reasonably sized chip.

To verify the sensitivity of the D-1 pixel design we illuminate the array with two monochromatic light sources: a HgAr lamp with 694 nm filter and a 982 nm laser. Pulses from these sources are shown in Figure 5 (Left) for a Q_m=54,000 pixel. The mean pulse height from 694 nm photons is ∼100°, however, it is worth noting that this is a higher Q_m pixel, so the phase offset for a given photon energy is greater than that expected for pixels with median Q_m. For pixels near the median Q_m we measure 694 nm pulse heights of ∼80°, matching the response of typical UV/optical tuned MKIDs to 254 nm photons[7] and demonstrating that our sensitivity is tuned as expected.

The energy resolution (R=E/ΔE) at a given wavelength is determined by the FWHM of a Gaussian fit to the pulse height distribution at that wavelength. We collect several thousand pulses from each light source, then fit the pulses with a template pulse that is used to generate a Weiner filter. We then make a histogram of the filtered pulse heights to evaluate the spread in pixel response to single wavelengths. Figure 5 (Right) shows an example of this analysis for 694 nm and 982 nm light measured by the same Q_m=54,000 pixel. We find a typical energy resolution R≈5 at 694 nm and R≈3 at 982 nm. This will improve as we move from engineering to science-grade arrays.

2.2.2 Array Layout

D-1 is composed of five identical 2000-pixel (80×25) segments with one feedline per segment. During fabrication (Section 2.2.3) each lithography step is performed by repeating the 2000-pixel mask one next to the other with a stepper to pattern a full D-1 chip. This strategy avoids the need for multiple photolithography masks (all fabrication layers would not fit on one mask if done at full D-1 scale), and could be expanded to scale arbitrarily in one dimension until we fill a 100 or 150 mm wafer.

The resonators in the 2000-pixel mask are designed to cover ∼4 GHz bandwidth with 1.8 MHz spacing between resonators and a 200 MHz gap between low and high frequency halves. Frequency tuning is accomplished by shortening pairs of interdigitated capacitor legs. At higher resonant frequencies the coupling bar must also be shortened to maintain Q_m=30,000 for all pixels. Otherwise, high frequency resonators will couple more effectively to the microwave transmission line and Q_m will decrease systematically with increasing frequency.

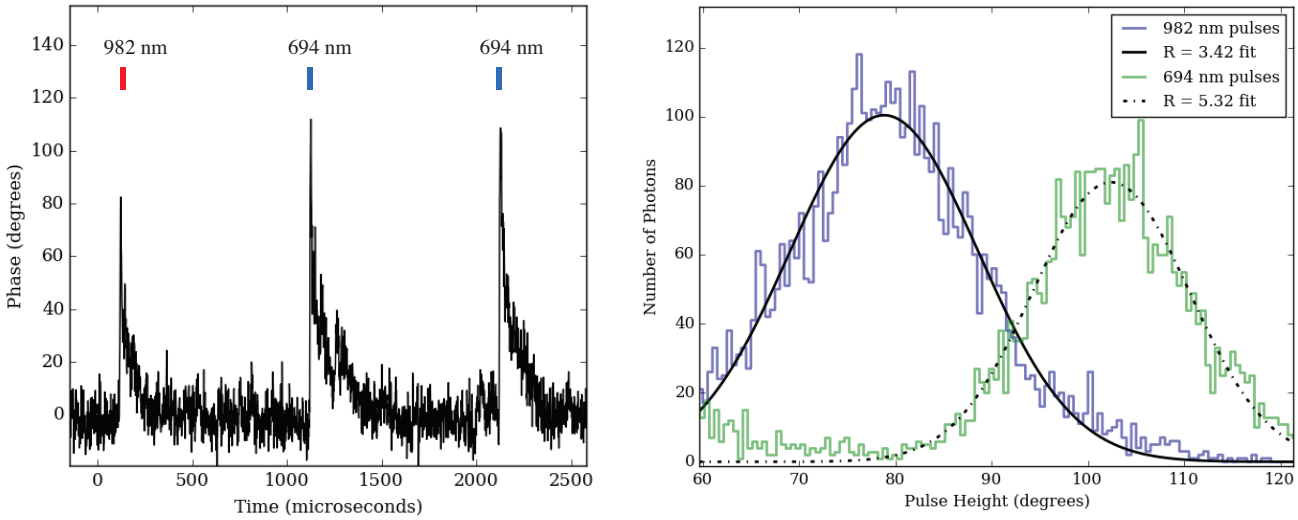

Figure 5. (Left) A phase time stream from a Q_m=54,000 D-1 pixel while being illuminated with 694 nm and 982 nm photons. Pulse height is defined as the maximum phase excursion, in degrees, measured by the microwave probe signal during a photon event, with more energetic photons resulting in greater pulse heights. (Right) Histogram of thousands of pulses from 694 nm and 982 nm light. By measuring the FWHM of the pulse height distribution in response to monochromatic light we determine the energy resolution (R=E/ΔE) of the MKID at that wavelength. For a typical engineering sample D-1 pixel we find R $\approx$ 5 at 694 nm and R $\approx$ 3 at 982 nm.

During array layout pixels are assigned to positions on the chip according to an algorithm that maximizes the physical distance between pixels with similar resonant frequencies to avoid cross-talk (nearest neighbors have Δf >50 MHz). This algorithm also takes into account a particular non-uniformity in the device fabrication: sputtered TiN can show large T_c gradients across a wafer,[30] which causes resonators to shift away from their design frequencies since $f \propto L^{-1/2}$ and $L \propto T_c^{-1}$ as described in the caption for Table 1. A frequency "collision" is defined as when two or more resonators land within 500 kHz of each other, such that we can no longer ensure that each unique readout tone is coupling to only a single pixel. These collisions are the dominant source of unusable pixels in our current arrays. The frequency map is optimized such that we always lose a predictable number of pixels due to collisions ($\sim$12$\pm$1%) regardless of randomly oriented T_c gradients.

In a full frequency sweep of one randomly selected feedline from our engineering-grade D-1 we find a raw pixel yield of 1750 resonators (87.5%). Another 275 pixels (13.7%) are lost due to frequency collisions, which is within 2σ of our predicted 12% collision rate, for a usable pixel yield of 1475 pixels (73.8%), roughly matching the total percent yield achieved with our previous instrument, ARCONS.[11]

Increasing feedline yield is a high priority in D-1. With ARCONS' MKID array (SCI-4) we encountered several fabrication defects that reduced our yield, most commonly caused by metallization steps that were not adequately etched, leaving enough metal behind to short the feedline center strip to the ground plane upon its deposition. Even a single small defect or scratch can render an entire feedline useless, and moving from a 2024-pixel, 2 feedline array to a 10,000-pixel, 5 feedline array will exacerbate this problem. In anticipation of this issue we re-oriented the pixels in D-1 and reflected them over either side of the feedline, effectively cutting each feedline length in half and reducing the odds of a defect breaking it. Figure 6 shows a side-by-side comparison of individual SCI-4 and D-1 pixels demonstrating this re-orientation. At this time there have not been enough D-1 arrays fabricated to quantify the yield improvement.

2.2.3 Fabrication

D-1 is fabricated in the Microdevices Lab at NASA's Jet Propulsion Laboratory (JPL). The fabrication procedure for D-1 closely follows that described in Mazin et al.[7] for achieving high quality TiN resonators on a high

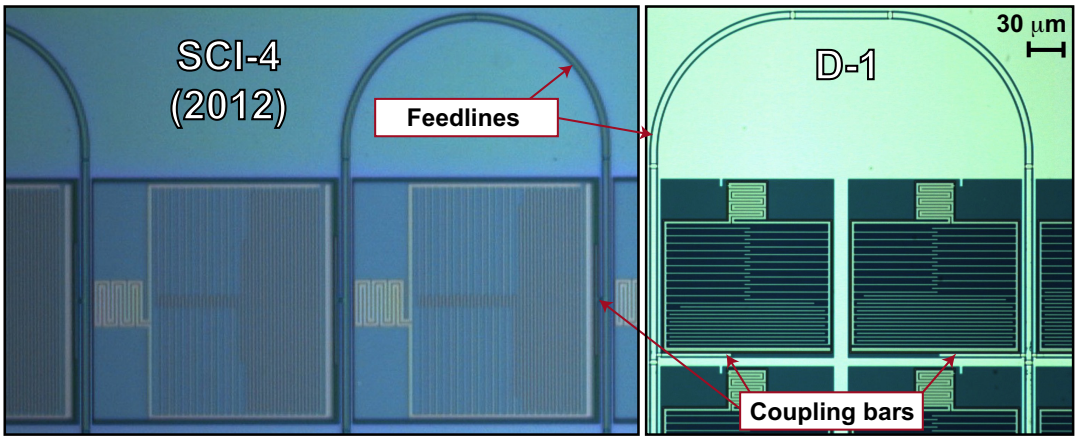

Figure 6. A comparison of individual pixels from the edges of the ARCONS SCI-4 array design and the D-1 array design. Both images are set to the same scale. The 90° reorientation allows D-1 pixels to be reflected over the feedline while keeping the inductors on the correct gridding for the microlens array. The result is that the feedline winds between every two columns of pixels for D-1, rather than every column as for SCI-4, effectively halving the total feedline length. This reorientation comes with an accompanying re-positioning of the coupling bars. Also evident in this comparison is the relatively smaller inductors required to tune D-1's sensitivity to lower energy photons as discussed in Section 2.2.1. Color differences between the two microscope images are not significant as both arrays are fabricated from the same materials.

resistivity Si substrate with a niobium (Nb) ground plane and CPW feedline, so we will only summarize recent improvements to the process here.

After depositing the TiN we etch it into a "resonator outline" pattern, leaving square TiN patches in the locations where resonators will be, but not yet etching the resonator slots. Fabrication then proceeds with the Nb transmission line, followed by SiO_2 cross-overs, and ground plane. An additional step is added to place gold bond pads around the border of the ground plane for improved heat sinking when wire-bonding the chip into its box. The final step is then to etch the resonator patterns into the TiN patches in a "cookie cutter" fashion. By breaking the resonator patterning into two steps this way, the TiN is still deposited on clean Si (a necessary precaution to achieve high quality resonators), and the fine resonator features are not created until the end of the process, ensuring they cannot be damaged or dirtied by the lift-off steps required for the Nb and gold.

2.3 Readout

The readout hardware and photon detection firmware for DARKNESS and MEC are structured very similarly to that of ARCONS, which is described in detail by McHugh et al.,[9] however, we have upgraded to the second generation of CASPER Reconfigurable Open-Architecture Computing Hardware (ROACH2) hardware[†]. Two digital-to-analog converters (DACs) generate signals for 1024 resonators at low frequencies, then send the signals through an intermediate frequency (IF) board for mixing up to our MKID frequencies spanning 2 GHz bandwidth. After passing through the cryostat the signals return through the IF board for down-conversion, then pass through two analog-to-digital converters (ADCs). The digitized signals are finally passed to the ROACH2 board where photon detection is done in firmware on a Virtex 6 Field Programmable Gate Array (FPGA). Using two board sets per feedline, covering 2 GHz each, requires the resonators on each feedline to operate between roughly 4-8 GHz, keeping all resonators within roughly an octave of readout bandwidth. For comparison ARCONS required eight ROACH boards for 2024 pixels whereas DARKNESS reads out 10,000 pixels per ten ROACH2 boards, a factor of 4 increase in readout density.

3. SIMULATED DARKNESS PERFORMANCE

We conducted simulations using the IDL wavefront propagation software, PROPER,[31] to estimate the contrast delivered by P1640 across DARKNESS's observing band. DARKNESS's optical design behind P1640 has been

[†]More details on ROACH2 can be found on the CASPER wiki: casper.berkeley.edu/wiki/ROACH2

finalized, and P1640 has been operating for several years, meaning we can compare our simulations against on-sky results from a well characterized instrument. While we expect higher contrast ratios from DARKNESS+SDC and MEC+SCExAO as these configurations will implement MKID focal plane wavefront control, neither SDC nor SCExAO is fully optimized yet and we do not have an empirical understanding of the ultimate contrast ratios they can achieve. Thus we limit our simulation to DARKNESS+P1640.

3.1 Simulated Contrast

We first simulated an unaberrated version of the Hale Telescope, P3K, and P1640 optical train with a uniform input beam and verified the accuracy of this model using Lyot plane images and contrast profiles provided in the P1640 design documentation.[‡] Aberrations were then added, with mirror phase errors approximated with power spectral density (PSD) error maps, using RMS values supplied in the P1640 documentation. Atmospheric turbulence and the AO loop were not simulated. Instead, a phase screen was applied to the coronagraph entrance beam with a 105 nm RMS amplitude to represent the residual wavefront error (WFE) delivered by the P3K AO system under median seeing, resulting in a simulated Strehl ratio of 85% at 1650 nm.[32] This method ignores any telescope or AO mirror aberrations, skipping straight to the corrected post-AO wavefront, which is attractive since it avoids guessing at the Hale 200" primary's aberrations that are not well characterized. Comparing with published results shows that the contrast curves presented here are not overly optimistic.[33,34]

With this framework in place we extend our simulations down through I-band, covering the entire DARKNESS bandwidth. Figure 7 shows contrast profiles with raw coronagraphic suppression, coronagraph+SDI, and coronagraph+Dark Speckle. SDI performance is approximated as an order of magnitude improvement in contrast, following Crepp et al.'s[15] results. Boccaletti et al.[20] provide a straightfoward analytical expression (Eqn. 5 in their paper) for estimating the SNR improvement due to Dark Speckle analysis, however, it is important to note that the statistical formulation used to derive this expression did not take static speckles into account. The curve presented here is for a SNR of 5 from a 3 hour total integration with 20 ms exposures, where G is given by the raw coronagraph contrast, $N_\star$ is calculated from known HR 8799 magnitudes with a 6% estimated system throughput, and j is given by the designed DARKNESS plate scale. It should be considered a lower limit where static speckles have been perfectly accounted for. When operating in unison SDI and Dark Speckle will certainly provide higher contrasts than either one is capable of alone since SDI will mitigate static speckles that would otherwise limit the utility of the Dark Speckle technique.[21] However, a deeper study of speckle statistics including static, quasistatic, and dynamic speckles is currently underway (Jensen-Clem et al., in prep.) with the intention of yielding a complete framework for speckle suppression incorporating statistical discrimination and chromatic information simultaneously.

3.2 Constraining HR 8799

To demonstrate the science potential of DARKNESS we have overplotted measured and simulated contrasts for the four planets around HR 8799[35,36] in Figure 7. We apply atmosphere models[37] to simulate the J-band photometry for HR 8799e and the I-band photometry for all four planets. Following Madhusudhan et al.[37] for the best-fitting models (and Skemer et al.[36] for HR 8799e) we apply simulated I and J-band filters and extract absolute magnitudes in each band. To estimate HR 8799's I-band magnitude we applied color tables scaled to the previously measured colors for HR 8799 (all roughly 2× those expected for a main sequence A5V star).[38] The simulated J-band contrast for HR 8799d and e places them just outside P1640's detectable regime, matching recent results from P1640 at this wavelength.[39] With the added suppression provided by DARKNESS, J-band spectral data can be reliably obtained for these objects from Palomar and compared against other recent measurements.[40]

The I-band contrast yields intriguing results. None of the planets are accessible with P1640 and SDI alone, even if the current detector was sensitive to those wavelengths. However, all planets are theoretically accessible with Dark Speckle imaging, given the current models' I-band magnitudes. Thus HR8799 provides an excellent test of DARKNESS's true capability, with the potential to place new spectral constraints on giant Exoplanet atmosphere models.

[‡]P1640 Design Document: www.astro.caltech.edu/∼shinkley/PROJECT_1640_files/P1640_DandO_compress.pdf

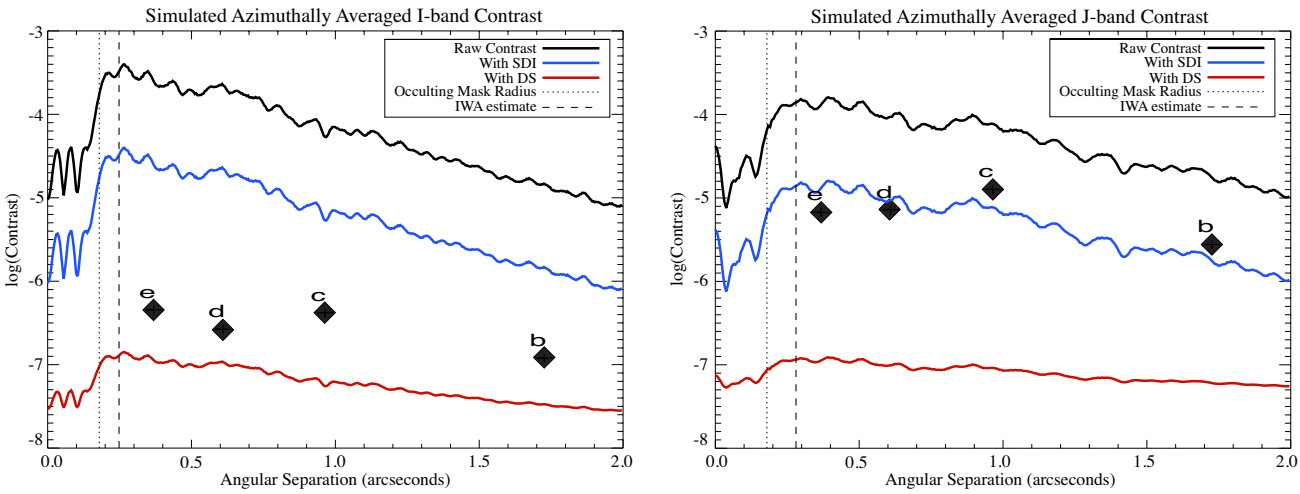

Figure 7. Simulated P1640 I and J-band contrast curves with 105 nm post-AO RMS wavefront error and aberrated coronagraph optics. HR 8799 planets are overplotted using available known photometry in J-band and photometry derived from model spectra in I-band (and J-band for planet e).[37] Spectral differential imaging (SDI) performance is estimated as an order of magnitude increase in contrast ratio, following Crepp et al.'s[15] results. 5-σ Dark Speckle (DS) suppression is estimated using Eqn. 5 from Boccaletti et al.[20] and should be considered a lower limit where static speckles have been perfectly accounted for. We find all planets should be detectable in both bands with DARKNESS, allowing us to place constraints on current atmosphere models should they be detected at the expected contrasts.

4. ONGOING DEVELOPMENT

Our group is actively developing the optical/near-IR MKID arrays used in DARKNESS and MEC. The D-1 array demonstrated here is a functioning engineering-grade array, but suffers from the same frequency collisions and lower-than-expected energy resolution we've experienced with ARCONS, both largely attributed to non-uniformities in the sputtered TiN film. We are making a concerted effort to identify new TiN fabrication techniques or entirely new superconducting materials that will improve these numbers.[41] Since DARKNESS is scheduled for commissioning in July 2016 (and MEC roughly 6 months later) there is the potential for any breakthroughs in our material development research to be incorporated into both instruments' MKID designs. Regardless of potential material breakthroughs, further refinement of the D-1 fabrication process will improve performance as well.

As mentioned in Section 2.1.3 the ITO coated window currently used for far-IR radiation blocking noticeably degrades the instrument throughput in the red end of our science bandpass. We are seeking alternative coatings or glasses to replace it before commissioning.

On the readout end, D-1 is currently read out in the lab using our existing ARCONS photon detection firmware, but this firmware is receiving several upgrades to take advantage of the extra resources provided with ROACH2. ARCONS firmware implemented a 100 μs dead-time between photon triggers to prevent detections of photons riding on the tails of previous ones, an effect that degrades energy resolution at high count rates (>1000 photons per second per pixel). However, as demonstrated with in-lab calibration data, degraded energy resolution is still found at high count rates despite this dead-time, and the dead-time introduces noticeable non-linearity in the measured count rates.[10,11] The firmware is currently being upgraded to better handle closely spaced photons with minimal dead-time to reduce these effects. DARKNESS and MEC's data output will be especially upgraded for speed to allow real-time processing and integration with the wavefront control systems at their respective telescopes. While ARCONS' readout software fills a 16 kB buffer with individual data packets and transfers data to the control computer whenever the buffer is half full, our upgraded readout software will pull all accumulated packets every 0.5 ms directly from the ROACH2 FPGAs to a dedicated analysis computer over 1-gigabit Ethernet. This fast processor will build up data cubes for focal plane feedback to the wavefront control system to perform speckle nulling.

ACKNOWLEDGMENTS

SRM and PS are supported by NASA Office of the Chief Technologist's Space Technology Research Fellowships (NSTRF). DARKNESS is funded by a National Science Foundation (NSF) ATI grant, number AST-1308556. MEC is funded by a National Astronomical Observatory of Japan (NAOJ) grant.

REFERENCES

[1] Hinkley, S., Oppenheimer, B. R., Zimmerman, N., et al. *PASP* **123**, 74–86 (Jan. 2011).
[2] Macintosh, B., Graham, J., Palmer, D., et al. *Proc. SPIE* **6272** (July 2006).
[3] Dohlen, K., Beuzit, J.-L., Feldt, M., et al. *Proc. SPIE* **6269** (July 2006).
[4] Martinache, F. and Guyon, O. *Proc. SPIE* **7440** (Aug. 2009).
[5] Jovanovic, N., Martinache, F., Guyon, O., et al. *ArXiv e-prints* (June 2015).
[6] Day, P. K., LeDuc, H. G., Mazin, B. A., et al. *Nature* **425**, 817–821 (Oct. 2003).
[7] Mazin, B. A., Bumble, B., Meeker, S. R., et al. *Optics Express* **20**, 1503 (Jan. 2012).
[8] Marsden, D., Mazin, B. A., Bumble, B., et al. *Proc. SPIE* **8453** (July 2012).
[9] McHugh, S., Mazin, B. A., Serfass, B., et al. *Rev. Sci. Inst.* **83**, 044702 (Apr. 2012).
[10] van Eyken, J. C., Strader, M. J., Walter, A. B., et al. *ApJS* **219**, 14 (July 2015).
[11] Mazin, B. A., Meeker, S. R., Strader, M. J., et al. *PASP* **125**, 1348–1361 (Nov. 2013).
[12] Strader, M. J., Johnson, M. D., Mazin, B. A., et al. *ApJL* **779**, L12 (Dec. 2013).
[13] Szypryt, P., Duggan, G. E., Mazin, B. A., et al. *MNRAS* **439**, 2765–2770 (Apr. 2014).
[14] Sparks, W. B. and Ford, H. C. *ApJ* **578**, 543–564 (Oct. 2002).
[15] Crepp, J. R., Pueyo, L., Brenner, D., et al. *ApJ* **729**, 132 (Mar. 2011).
[16] Fergus, R., Hogg, D. W., Oppenheimer, R., et al. *ApJ* **794**, 161 (Oct. 2014).
[17] Aime, C. and Soummer, R. *ApJL* **612**, L85–L88 (Sept. 2004).
[18] Fitzgerald, M. P. and Graham, J. R. *ApJ* **637**, 541–547 (Jan. 2006).
[19] Labeyrie, A. *A&A* **298**, 544 (June 1995).
[20] Boccaletti, A., Labeyrie, A., and Ragazzoni, R. *A&AS* **338**, 106–110 (Oct. 1998).
[21] Boccaletti, A., Moutou, C., and Abe, L. *A&AS* **141**, 157–164 (Jan. 2000).
[22] Gladysz, S. and Christou, J. C. *ApJ* **684**, 1486–1495 (Sept. 2008).
[23] Gladysz, S. and Christou, J. C. *ApJ* **698**, 28–42 (June 2009).
[24] Malbet, F., Yu, J. W., and Shao, M. *PASP* **107**, 386 (Apr. 1995).
[25] Martinache, F., Guyon, O., Jovanovic, N., et al. *PASP* **126**, 565–572 (June 2014).
[26] Hayward, T. L., Brandl, B., Pirger, B., et al. *PASP* **113**, 105–118 (Jan. 2001).
[27] Hinkley, S., Oppenheimer, B. R., Brenner, D., et al. *Proc. SPIE* **7015** (July 2008).
[28] Zmuidzinas, J. *Annu. Rev. Condens. Matter Phys.* **3**, 169–214 (Mar. 2011).
[29] Roquiny, P., Bodart, F., and Terwagne, G. *Surface and Coatings Technology* **116**, 278 (Sept. 1999).
[30] Vissers, M. R., Gao, J., Sandberg, M., et al. *APL* **102**, 232603 (June 2013).
[31] Krist, J. E. *Proc. SPIE* **6675** (Sept. 2007).
[32] Dekany, R., Roberts, J., Burruss, R., et al. *ApJ* **776**, 130 (Oct. 2013).
[33] Cady, E., Baranec, C., Beichman, C., et al. *Proc. SPIE* **8864** (Sept. 2013).
[34] Oppenheimer, B. R., Beichman, C., Brenner, D., et al. *Proc. SPIE* **8447** (July 2012).
[35] Marois, C., Macintosh, B., Barman, T., et al. *Science* **322**, 1348– (Nov. 2008).
[36] Skemer, A. J., Hinz, P. M., Esposito, S., et al. *ApJ* **753**, 14 (July 2012).
[37] Madhusudhan, N., Burrows, A., and Currie, T. *ApJ* **737**, 34 (Aug. 2011).
[38] Zombeck, M., [*Handbook of Space A&A: Third Edition*], Cambridge University Press (2007).
[39] Oppenheimer, B. R., Baranec, C., Beichman, C., et al. *ApJ* **768**, 24 (May 2013).
[40] Zurlo, A., Vigan, A., Galicher, R., et al. *ArXiv e-prints* (Nov. 2015).
[41] Szypryt, P., Mazin, B. A., Bumble, B., et al. *IEEE* **25** (June 2015).